Mechanical Fragmentation of Wheat Straw at Different Plant Scales: Pb^{2+} Adsorption Behavior and Mechanism

Yaoyao Cao, Weihua Xiao, Guanghui Shen, Guanya Ji, Yang Zhang, Chongfeng Gao, and Lujia Han *

Wheat straw samples at the plant scale (> 1 mm), tissue scale (100 to 500 μm), and cellular scale (30 to 50 μm) were produced to characterize their microstructure and adsorption properties. The effects of changes in the microstructure and adsorption properties on the adsorption capacity of Pb^{2+} were investigated. The results implied that specific surface areas and pore volumes in the cellular-scale sample were four to five times larger than at other scales, as superfine grinding destroyed the structure of tissues and cell walls. The crystallinity declined significantly from 53% to 34% with decreasing fragmentation scale. Changes in adsorption properties (point of zero charge, acidic functional groups, and cation exchange capacity) were not apparent. The pseudo-second-order model and Langmuir isotherm model fit the experimental data better than alternate models. The adsorption capacity of Pb^{2+} increased significantly with decreasing fragmentation scale. The main mechanism improving the adsorption capacity of Pb^{2+} was intensive complexation owing to an increase in cellulose accessibility to water and enhanced chemical reaction activity of the hydroxyl groups, rather than physical and electrostatic adsorption.

Contact information: Laboratory of Biomass and Bioprocessing Engineering, College of Engineering, China Agricultural University, P. O. Box 191, 17 Qinghua Donglu, Beijing 100083, China;
* Corresponding author: hanlj@cau.edu.cn

INTRODUCTION

The rapid pace of industrial activity is increasingly contributing to serious environmental pollution. The presence of heavy metals in effluents has detrimental effects on human health and the environment due to their non-biodegradable, highly toxic, and bioaccumulating nature. Among various metal ions, lead, mercury, cadmium, and chromium are the most toxic (Tan and Xiao 2009; Farooq *et al*. 2010). Conventional treatment methods include chemical precipitation, electrolysis, and membrane filtration, which have disadvantages such as high cost, high energy input, and secondary pollution (Farooq *et al*. 2011; Ding *et al*. 2012). Hence, finding an optimal technology that is both cost effective and efficient is vital.

Biosorption describes the removal of heavy metals by biological materials (Salman *et al*. 2015), which are available in large quantities, are easy to operate, and can be regenerated (Farooq *et al*. 2010; Ding *et al*. 2012; Pandi and Viswanathan 2015). Various materials have been employed as adsorbents, such as straw (Tan and Xiao 2009; Gorgievski *et al*. 2013), saw dust (Kalavathy and Miranda 2010), biomass-derived biochar (Rao *et al*. 2008; Wang *et al*. 2015), and algae (Gupta *et al*. 2001). However, the

biosorption mechanisms of heavy metals are complicated, and mainly include physical adsorption, electrostatic adsorption, cation exchange, and complexation (Demirbas 2008; Robalds *et al*. 2016). Physicochemical properties of the adsorbent, such as particle size, surface area, and surface functional groups, have different effects on adsorption efficiency (Benhima *et al*. 2008; Mishra *et al*. 2010; Fomina and Gadd 2014). Benhima *et al*. (2008) reported the adsorption capacity of Pb^{2+} onto *Euphorbia echinus* and *Carpobrotus edulis* for particle sizes of 200 to 500 μm, 50 to 200 μm, and < 50 μm. The maximum metal uptake was obtained with particles < 50 μm, indicating that adsorption capacity can be improved by reducing the median particle size. Mishra *et al*. (2010) found that the adsorption efficacy of Zn^{2+} ions onto eucalyptus bark saw dust, mango bark saw dust, and pineapple fruit peel depends on particle size, surface structure, and the functional groups involved.

Straw is an important biomass feedstock with enormous worldwide production and a wide geographic distribution (Zhang *et al*. 2016; Gao *et al*. 2017). Ji *et al*. (2016) and Zhang *et al*. (2016) found that the microstructural features and physicochemical characteristics of straw samples were significantly influenced by different mechanical fragmentation scales. Therefore, it is crucial to explore the impact of microstructural and physicochemical properties at different plant scales on heavy metal adsorption.

In this study, the microstructure and adsorption properties of wheat straw at different plant scales were systematically characterized. The effects of changes in microstructure and adsorption properties on the adsorption capacity of Pb^{2+} were investigated to analyze adsorption mechanisms. Thus, we establish an important foundation for improving the adsorption capacity of wheat straw and elucidating Pb^{2+} adsorption mechanisms.

EXPERIMENTAL

Preparation of Wheat Straw Samples at Different Plant Scales

Wheat straw was collected from Beijing in 2015. The moisture of the wheat straw was 4.11 to 4.98%. According to the National Renewable Energy Laboratory method (Sluiter *et al*. 2010), the chemical composition of the wheat straw (dry basis) was 32.79% to 34.72% cellulose, 16.33% to 17.61% hemicellulose, 22.99% to 25.27% lignin, 17.85% to 18.40% starch, 4.14% to 4.62% protein and a small amount of other substances such as lipid and pectin.

First, raw wheat straw was cut into 3 to 5 cm pieces and sheared to approximately 1 cm, and the obtained control sample was denoted as CK (plant scale). The prepared 3 to 5 cm samples were coarsely milled using an RT-34 milling machine (Hongquan Pharmaceutical Machinery Ltd., Hong Kong, China) by passing them through a 1.00-mm screen and using a sieved-based mill ZM200 (Retsch, Haan, Germany) by passing them through a 0.50 mm screen. The two obtained samples were denoted as IM1.00 (tissue scale) and IM0.50 (tissue scale), respectively. Lastly, an ultrafine vibration ball mill CJM-SY-B (Qinghuangdao Taiji Ring Nano Ltd., Hebei, China) was used to produce the cellular-scale sample, and a cooling water system was used to control the milling process below 30 °C. Then, 70 g of IM1.00 tissue samples and 2800 g of ZrO_2 balls (6 to 10 mm diameter) were mixed in a 2-L tank for 30 minutes, and the produced sample was denoted as BM.

The prepared wheat straw samples were oven-dried to a constant weight at 45 °C, and stored in sealed bags.

Microstructure Characteristics of Wheat Straw Samples at Different Plant Scales

Particle size distribution

A Mastersizer 3000 laser diffraction particle analyzer (Malvern Instruments Ltd., Great Malvern, UK) was used to determine particle size in the range of 0.01 to 3000 μm by dispersing the wheat straw samples in air. The parameters D_{10}, D_{50}, and D_{90} represent the 10th, 50th, and 90th percentiles of the total volume, respectively, and D_{50} is the median particle size. Each sample was determined in triplicate.

Scanning electron microscopy (SEM)

A small amount of wheat straw sample was put on the sample stage for sputter treatment with platinum, and an S-4800 field-emission scanning electron microscope (Hitachi Ltd., Tokyo, Japan) was utilized to observe the structural characteristics and compare the differences in morphology between wheat straw samples at different plant scales.

Specific surface areas (SSA) and pore volumes (PV)

Wheat straw samples (degassed for 4 h at 105 °C) were measured by an ASAP 2020 Plus Physisorption device (Micromeritics Instruments Ltd., Norcross, USA). The Brunauer-Emmett-Teller (BET) and Barrett-Joyner-Halenda (BJH) methods were applied to calculate the specific surface areas and pore volumes, respectively. Each sample was determined in duplicate.

Crystallinity

The crystallinity of wheat straw samples was analyzed by a D8 ADVANCE X-ray diffractometer (XRD) (Bruker, Karlsruhe, Germany) with Cu-Kα at 40 kV and 30 mA. The operating conditions were 2θ ranged 5° to 40° at a rate of 2°/min in 0.02° increments. Each sample was determined in duplicate. The cellulose crystallinity index (CrI) was calculated as follows (Segal *et al*. 1959),

$$CrI\ (\%) = \frac{I_{002} - I_{am}}{I_{002}} \times 100 \qquad (1)$$

where I_{002} is the maximum diffraction peak intensity; and I_{am} is the diffraction peak intensity at approximately $2\theta = 18.0°$, namely amorphous zone diffraction.

Infrared spectroscopy

Attenuated total reflectance-Fourier transform infrared spectroscopy (ATR-FTIR) spectra were obtained using a TENSOR II Fourier transform infrared spectrometer (Bruker, Karlsruhe, Germany) in the range of 4000 to 400 cm^{-1} with 32 times scan and resolution of 4 cm^{-1}. Each sample was determined in triplicate.

Adsorption Properties of Wheat Straw Samples at Different Plant Scales

Acidic functional groups (AFG)

Lignocellulosic biomass has the potential to adsorb heavy metals due to the covalent bond between metal ions and acidic functional groups at the surface (Abdolali *et al*. 2014; Salman *et al*. 2015). Among them, carboxylic groups and phenol hydroxyl groups can combine with Pb^{2+} in their chemical compound (Feng *et al*. 2009; Al-Ghouti *et al*.

2010). The contents of acidic functional groups in wheat straw can be analyzed by the Boehm titration method (Boehm 1966). The measurement process comprised the following steps: 0.1 g of wheat straw was placed into 25 mL of 0.01 M NaOH solution for 1 h at 25 °C and 150 rpm. Then, 10 mL of supernatant was titrated by 0.01 M HCl to obtain the consumption concentrate of NaOH and determine the total acidic functional group content. Each sample was determined in triplicate.

Cation exchange capacity (CEC)

Cation exchange capacity (CEC) is used to evaluate the ability of materials to adsorb positive ions (Gorgievski *et al*. 2013). The adsorption of heavy metals involves cation exchange interaction, as well as other mechanisms such as physical adsorption, electrostatic adsorption, and complexation (Demirbas 2008). To some extent, the cation exchange capacity reflects the adsorption capacity of the adsorbent, but it is not the unique determining factor (Shen *et al*. 2017). The measurement process was as follows: 1 g of wheat straw and 50 mL of 0.01 M NH_4Cl solution were added to an Erlenmeyer flask and kept at 25 °C and 300 rpm for 24 h. Then, the supernatant was filtered using a 0.45-μm membrane, and a NexION 300 ICP-MS (PE, US) was used to determine the concentrations of Na^+, Mg^{2+}, K^+ and Ca^{2+} (Gorgievski *et al*. 2013). Each sample was determined in triplicate.

Experimental Methods and Measurements

According to optical adsorption experiments (Dang *et al*. 2009; Ding *et al*. 2012; Gorgievski *et al*. 2013), 0.5 g of wheat straw was added to Pb^{2+} aqueous solution (25 mL, pH = 5.0) at 25 °C and 150 rpm for a period of time. The suspension was filtered and measured using a Vario 6 series atomic absorption spectrometer (Analytik Jena, Jena, Germany). Each sample was determined in triplicate.

The amount of Pb^{2+} adsorbed per unit mass of wheat straw (q_e) was calculated from the following equation.

$$q_e = \frac{C_o - C_e}{W} V \qquad (2)$$

where C_o and C_e are the initial and equilibrium Pb^{2+} concentrations (mg/L), respectively. V and W are the volume of the Pb^{2+} solution (L) and the mass of wheat straw (g), respectively.

Adsorption kinetics

A Pb^{2+} adsorption experiment was carried out to evaluate adsorption kinetics. 0.5 g of wheat straw was added to 100 mg/L Pb^{2+} aqueous solution (25 mL, pH = 5.0) at 25 °C, 150 rpm, and the reaction time was set at 1, 3, 5, 10, 15, 20, 30, 60, 120, 180, and 240 min.

Generally, the pseudo-first-order model assumes the reaction rate is a linear function of the concentration of the reactant and is determined by a single factor. The expression is as follows:

$$\frac{d_q}{d_t} = K_1 (q_e - q_t) \qquad (3)$$

$$q_t = q_e(1 - e^{-K_1 t}) \qquad (4)$$

The pseudo second order model is given as follows,

$$\frac{d_q}{d_t} = K_2 \, (q_e - q_t)^2 \tag{5}$$

$$q_t = \frac{q_e{}^2 K_2 t}{1 + q_e K_2 t} \tag{6}$$

where q_e and q_t are the amount of Pb^{2+} adsorbed per unit mass of wheat straw at equilibrium and time t (mg/g), respectively. K_1 and K_2 are the rate constants of pseudo-first-order adsorption (min^{-1}) and pseudo-second-order adsorption (g/(mg• min)), respectively.

Adsorption isotherms

Another Pb^{2+} adsorption experiment was carried out to investigate adsorption isotherms. 0.5 g of wheat straw was added to Pb^{2+} aqueous solution (25 mL, pH = 5.0) at 25 °C, 150 rpm for 180 min. Initial Pb^{2+} concentrations were 100, 200, 300, 500, 1000, 1500, and 2000 mg/L.

The Langmuir model assumes that the surface of the adsorbent is homogeneous and the adsorbate molecule or atom can only occupy one surface site (Hubbe *et al*. 2011). The Langmuir model is suitable for monolayer adsorption with the following equations:

$$q_e = \frac{q_m K_L C_e}{1 + K_L C_e} \tag{7}$$

$$R_L = \frac{1}{1 + K_L C_o} \tag{8}$$

The Freundlich model can be expressed as follows,

$$q_e = K_F \, C_e{}^{1/n} \tag{9}$$

where q_e is the amount of Pb^{2+} adsorbed per unit mass of wheat straw at equilibrium (mg/g) and q_m is the maximum amount of Pb^{2+} adsorbed per unit mass of wheat straw (mg/g). C_o and C_e are the initial and equilibrium Pb^{2+} concentrations (mg/L), respectively. K_L is the isothermal adsorption equilibrium constant to describe the affinity of the binding site. R_L is the equilibrium parameter: $0 < R_L < 1$ indicates the adsorption reaction is prone to occur; $R_L > 1$ indicates the adsorption reaction is difficult to carry out; $R_L = 0$ indicates the adsorption reaction is irreversible; $R_L = 1$ indicates the adsorption is reversible. K_F is the Freundlich isothermal adsorption equilibrium constant; the larger the K_F value, the stronger the binding force between the adsorbent and adsorbate. *1/n* represents adsorption intensity; it is generally considered that $0 < 1/n < 1$ indicates a preferential adsorption process; $1/n > 2$ indicates the adsorption reaction is difficult to carry out.

Na^+, Mg^{2+}, K^+ and Ca^{2+} released during Pb^{2+} adsorption

0.5 g of wheat straw was added to 100 mg/L Pb^{2+} aqueous solution (25 mL, pH = 5.0) at 25 °C, 150 rpm for 180 min. A NexION 300 ICP-MS device (PE, US) was used to determine the concentrations of Na^+, Mg^{2+}, K^+ and Ca^{2+} in the wheat straw samples before and after adsorption. Each sample was determined in duplicate.

Statistical Analysis

Statistical tests were performed using the analysis of variance (ANOVA) with Duncan's multiple-range tests. Statistical data analysis was conducted using SPSS 20.0 (IBM Corporation, Armonk, New York, USA).

RESULTS AND DISCUSSION

Microstructural Character of Wheat Straw Samples at Different Plant Scales

The changes in microstructural characteristics of wheat straw at different plant scales are shown in Figs. 1 through 5, Table 1 and Table 2.

The peaks of the particle size distribution curves for IM1.00, IM0.50, and BM were shifted to the left, revealing a decrease in particle size (Fig. 1). The median particle size (D_{50}) of CK was 1 cm (plant scale), the D_{50} values for IM1.00 and IM0.50 were in the range of 100 to 500 µm (tissue scale), and the D_{50} of BM was only 10.53 µm (cellular scale, Table 1); thus, there were statistically significant differences in D_{50} among the wheat straw samples at different plant scales.
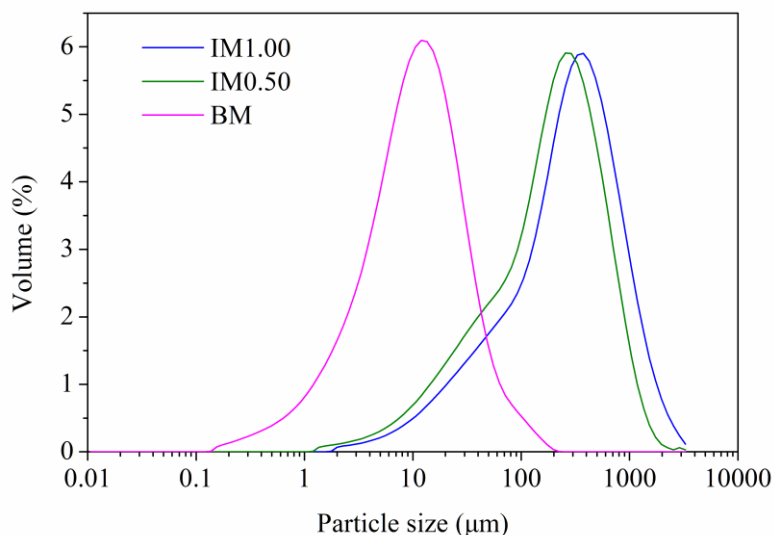
Fig. 1. Particle size distribution of wheat straw samples at different plant scales
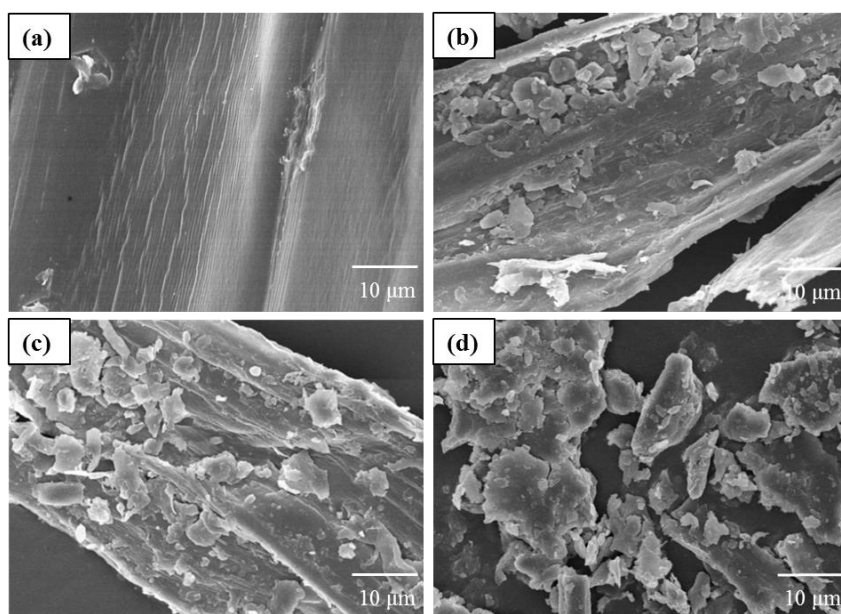
Fig. 2. SEM images of wheat straw samples at different plant scales. (a) CK, (b) IM1.00, (c) IM0.50, and (d) BM

The SEM images show an intact fibrous structure of CK with a smooth and dense

surface (Fig. 2). The damaged IM1.00 and IM0.50 became rough, tended to desquamate, and exposed the interior vascular bundle structure. While wheat straw fragmented to the cellular scale, there was no obvious fiber structure in the SEM diagram of BM, and powders were shaped as a cluster of irregular granular particles (Zhang *et al*. 2017).

The specific surface areas (SSA) and pore volumes (PV) of wheat straw samples at different plant scales are shown in Table 1. The SSA of CK, IM1.00, IM0.50, and BM were 0.46 ± 0.08, 0.67 ± 0.17, 0.78 ± 0.37, and 2.63 ± 0.18 m^2/g, respectively, and the PV were $(2.16 \pm 0.13) \times 10^{-3}$, $(2.81 \pm 1.33) \times 10^{-3}$, $(3.09 \pm 1.44) \times 10^{-3}$, and $(14.92 \pm 0.87) \times 10^{-3}$ cm^3/g, respectively. The SSA and PV in sample BM were significantly greater than at other scales. The SSA of a particle is composed of the exterior specific area, largely determined by particle size, and the interior surface area, influenced by porosity (Benhima *et al*. 2008; Zhang *et al*. 2016). In this study, since the increase of SSA in wheat straw samples was remarkably lower than the reduction of particle size, the interior specific surface area contributed a greater percentage to the overall SSA for wheat straw samples. In addition, BM had mainly large pores (> 50 nm) and mesopores (2 to 50 nm), while the pores of other scales were mainly mesoporous structures (Fig. 3). When the external pressure was higher than the internal pressure of the fibers in the superfine grinding, the internal closed pores were destroyed to form an open structure, which enlarged pore sizes and pore volumes (Wang *et al*. 2014).

Cellulose, one of the main components in wheat straw, contains orderly arrangements of crystalline regions and irregular amorphous structures (Ji *et al*. 2016). Crystalline peaks of 101, 10$\bar{1}$, 002, and 040 can be observed near $2\theta = 16°$, $22°$, and $35°$ in the X-ray diffraction (XRD) spectra (Gong *et al*. 2016; Ji *et al*. 2016). At $2\theta = 22°$, the intensity of the maximum diffraction peak was the highest in CK, while it weakened gradually from IM1.00 to IM0.50 and finally BM (Fig. 4), demonstrating that mechanical fragmentation destroyed the crystalline region of cellulose. Differences in the cellulose crystallinity index (CrI) of wheat straw samples at different plant scales are shown in Table 2. For plant-scale samples, the CrI of CK was 53%. After mechanical fragmentation at the tissue scale, the CrI values declined to 46% for IM1.00 and 45% for IM0.50. With the particle size decreased to the cellular scale, the CrI was only 34% in BM.
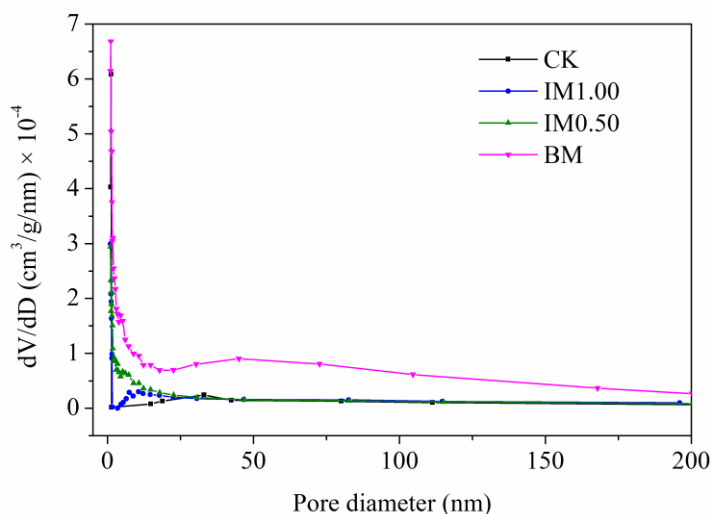
Fig. 3. Pore volume versus pore diameter for wheat straw samples at different plant scales

The crystallinity decreased significantly with decreasing particle size. As the

mechanical fragmentation scales decreased, the cellulose chain was damaged as hydrogen bonds were broken; thus, the crystallinity of the wheat straw samples was reduced (Silva *et al.* 2012; Ji *et al.* 2016).
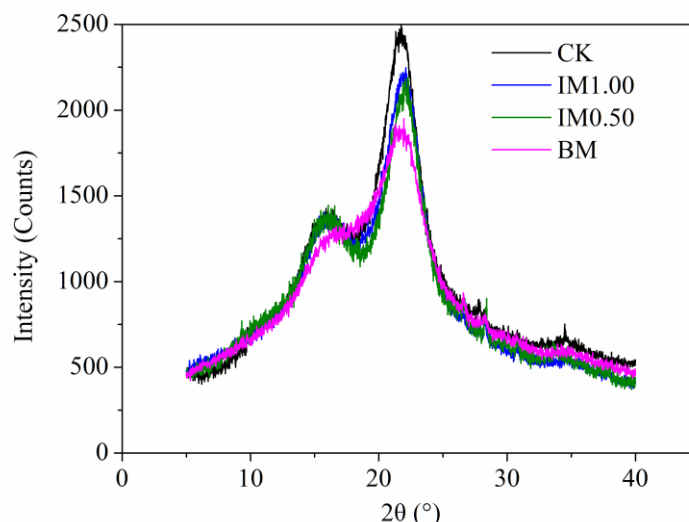
Fig. 4. XRD patterns of wheat straw samples at different plant scales

Table 1. Microstructural Characteristics of Wheat Straw Samples at Different Plant Scales

		CK	IM1.00	IM0.50	BM
Particle size[e]	D_{10} (µm)	ND	35.03 ± 1.46[c]	31.97 ± 1.50[b]	2.06 ± 0.02[a]
	D_{50} (µm)	10000 ± 500[d]	328.33 ± 11.37[c]	257.33 ± 4.04[b]	10.53 ± 0.06[a]
	D_{90} (µm)	ND	947.33 ± 23.46[c]	839.33 ± 43.75[b]	35.67 ± 0.87[a]
SSA (m²/g)		0.46 ± 0.08[a]	0.67 ± 0.17[a]	0.78 ± 0.37[a]	2.63 ± 0.18[b]
PV (×10⁻³, cm³/g)		2.16 ± 0.13[a]	2.81 ± 1.33[a]	3.09 ± 1.44[a]	14.92 ± 0.87[b]
CrI (%)		52.94 ± 3.70[c]	45.56 ± 2.39[b]	44.83 ± 0.49[b]	33.96 ± 1.31[a]

Notes: [a-d] Indicates that values in the same row are significantly different ($p < 0.05$).
[e] Particle size data are shown as their triplicate mean ± standard deviation.
ND: not detected. Data are shown as their duplicate mean ± standard deviation.

The ATR-FTIR change analysis of wheat straw samples at different scales is shown in Fig. 5 and Table 2. The absorption band near 3336 cm⁻¹ is assigned to O-H group stretching due to cellulose, hemicellulose, lignin, and pectin (Ibrahim *et al.* 2011). The stretching vibration of C=O at 1733 cm⁻¹ is attributed to the presence of carboxyl and ester groups in hemicellulose, pectin, and lipid (Himmelsbach *et al.* 2002). 1604 cm⁻¹ and 1507 cm⁻¹ are the characteristic of aromatic rings, which are considered to be the characteristic absorption peaks of lignin (Ibrahim *et al.* 2011; Liu *et al.* 2013; Yuan *et al.* 2015). At 898 cm⁻¹, the characteristic peak corresponding to C-H in cellulose was increased, which was due to the hydrogen bonding in the cellulose chain being broken and the decreased ratio of crystalline regions, and the result was consistent with the XRD crystallinity measurements.
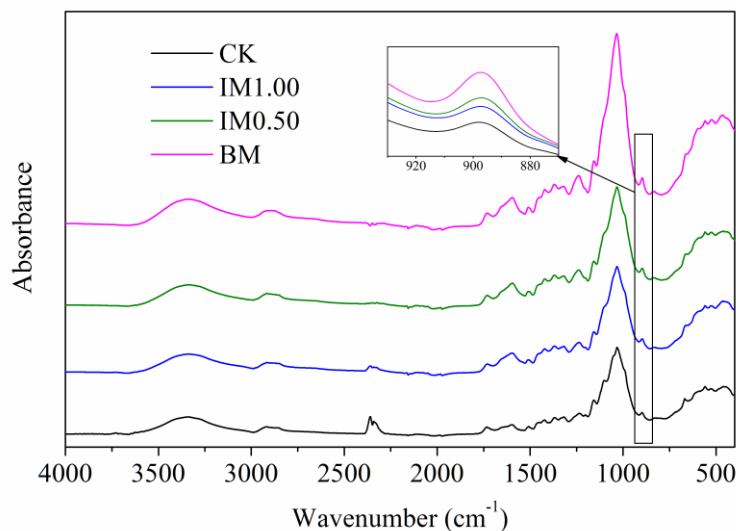
Fig. 5. ATR-FTIR change analysis of wheat straw samples at different scales

Table 2. Major Absorption Peaks in Infrared Spectra of Wheat Straw Samples at Different Scales

CK	IM1.00	IM0.50	BM	Assignment
Wavenumber (cm^{-1})				
3336	3338	3338	3338	O-H stretching
2917	2916	2916	2895	CH/CH$_2$ stretching
1733	1731	1731	1731	C=O stretching
1604	1599	1596	1595	aromatic skeletal vibration
1507	1510	1511	1509	aromatic skeletal stretching
1424	1422	1421	1421	CH$_2$ and CH symmetric bending
1367	1369	1369	1370	CH deformation/OH bending
1317	1319	1319	1319	C-H bending
1234	1238	1238	1240	C-O stretching
1157	1157	1157	1157	C-O stretching
1032	1033	1033	1034	C-O stretching
898	897	897	897	C-H stretching

Adsorption Properties of Wheat Straw Samples at Different Plant Scales

The adsorption properties of wheat straw samples at different plant scales are shown in Table 3. The acidic functional group (AFG) values of CK, IM1.00, IM0.50, and BM were 1.25 ± 0.04, 1.43 ± 0.03, 1.46 ± 0.03, and 1.53 ± 0.06 mmol/g. The AFG value of the cellular-scale sample was significantly higher than that of the plant-scale sample; while there were no significant differences among the cellular and tissue scales. Therefore, the influence of mechanical fragmentation scales on acidic functional groups was extremely limited. The cation exchange capacity (CEC) of wheat straw samples increased in the order: CK < IM1.00 < BM < IM0.50. From plant to tissue scale, the CEC of wheat straw samples increased significantly, which could be viewed as the result of increasing cation exchange with ammonium ions due to tissue structure destruction by mechanical fragmentation. However, the CEC of the cellular-scale sample was significantly less than that of the tissue sample IM0.50. This phenomenon indicates that the cation exchange capacity was incapable of increasing at the cellular scale if the fragmentation scale was further reduced by superfine grinding.

Table 3. Adsorption Properties of Wheat Straw Samples at Different Plant Scales

		CK	IM1.00	IM0.50	BM
AFG (mmol/g)		1.25 ± 0.04[a]	1.43 ± 0.03[b]	1.46 ± 0.03[b]	1.53 ± 0.06[b]
CEC (meq/g)	Na^+	0.0957 ± 0.0031[a]	0.0900 ± 0.0111[a]	0.0952 ± 0.0012[a]	0.1111 ± 0.0188[a]
	Mg^{2+}	0.0873 ± 0.0061[a]	0.1550 ± 0.0011[bc]	0.1551 ± 0.0035[c]	0.1388 ± 0.0065[b]
	K^+	0.3641 ± 0.0218[a]	0.4846 ± 0.0254[b]	0.6372 ± 0.0163[c]	0.4974 ± 0.0471[b]
	Ca^{2+}	0.1131 ± 0.0111[a]	0.1496 ± 0.0082[b]	0.1814 ± 0.0079[c]	0.1351 ± 0.0050[ab]
	Total	0.6602 ± 0.0421[a]	0.8743 ± 0.0435[b]	1.0688 ± 0.0036[c]	0.8824 ± 0.0300[b]

Notes: Data are shown as their triplicate mean ± standard deviation.
[a-c] Indicates that values in the same row are significantly different ($p < 0.05$).

Adsorption Kinetics and Isotherms of Pb^{2+}

Adsorption kinetics

The adsorption capacity of Pb^{2+} onto wheat straw samples at different plant scales at different adsorption reaction time is shown in Fig. 6 and Table 4. The adsorption capacity of Pb^{2+} onto plant scale and tissue scale samples increased rapidly and then plateaued with increasing adsorption time, while the adsorption capacity of Pb^{2+} onto wheat straw at cellular scale reached adsorption equilibrium in the initial period. In this study, 180 min was chosen to be the adsorption equilibrium time, as it was sufficient to ensure reaching the equilibrium adsorption capacity of Pb^{2+}. As shown in Fig. 7 and Table 5, the experimental data was fitted using the pseudo-first-order model, and the adsorption equilibrium was reached quickly, which resulted in a fast adsorption rate and deviation between modeled equilibrium adsorption capacity and experimental values. Meanwhile, all the coefficients of determination (R^2) of the pseudo-second-order model were higher than 0.95, and equilibrium adsorption capacity of Pb^{2+} obtained at equilibrium was closer to the respective experimental values. Particularly, the adsorption rate (K_2) of BM was 45 times higher than that of other samples, which indicated that superfine grinding increased the available Pb^{2+} adsorption sites by reducing the particle size of wheat straw at the cellular scale. Therefore, the adsorption reaction rate was accelerated, and adsorption equilibrium could be reached quickly.
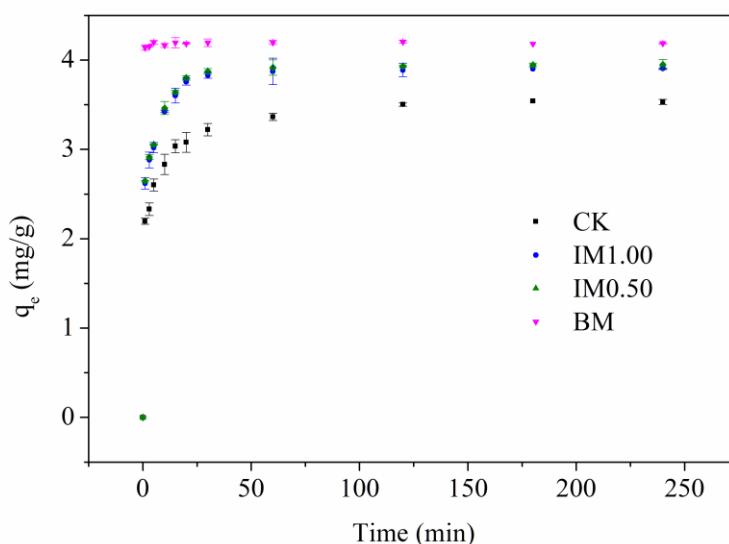
Fig. 6. Adsorption capacity of Pb^{2+} onto wheat straw samples at different plant scales at different adsorption reaction time

Table 4. Adsorption Capacity of Pb^{2+} onto Wheat Straw Samples at Different Plant Scales at Different Adsorption Reaction Time

Time (min)	CK	IM1.00	IM0.50	BM
1	2.20 ± 0.04[a]	2.62 ± 0.06[b]	2.65 ± 0.00[b]	4.14 ± 0.03[c]
3	2.33 ± 0.07[a]	2.88 ± 0.08[b]	2.92 ± 0.02[b]	4.15 ± 0.01[c]
5	2.60 ± 0.07[a]	3.02 ± 0.06[b]	3.06 ± 0.01[b]	4.20 ± 0.02[c]
10	2.83 ± 0.11[a]	3.43 ± 0.01[b]	3.46 ± 0.07[b]	4.17 ± 0.02[c]
15	3.04 ± 0.08[a]	3.60 ± 0.08[b]	3.65 ± 0.02[b]	4.19 ± 0.06[c]
20	3.08 ± 0.11[a]	3.76 ± 0.04[b]	3.80 ± 0.03[b]	4.19 ± 0.01[c]
30	3.22 ± 0.07[a]	3.83 ± 0.03[b]	3.87 ± 0.03[b]	4.19 ± 0.04[c]
60	3.36 ± 0.04[a]	3.88 ± 0.15[b]	3.92 ± 0.08[b]	4.20 ± 0.02[c]
120	3.50 ± 0.01[a]	3.89 ± 0.08[b]	3.93 ± 0.01[b]	4.20 ± 0.01[c]
180	3.54 ± 0.00[a]	3.90 ± 0.00[b]	3.95 ± 0.02[c]	4.18 ± 0.00[d]
240	3.53 ± 0.03[a]	3.91 ± 0.01[b]	3.95 ± 0.06[c]	4.19 ± 0.01[d]

Notes: Data are shown as their triplicate mean ± standard deviation.
[a-d] Indicates that values in the same row are significantly different ($p < 0.05$).

(a)

(b)
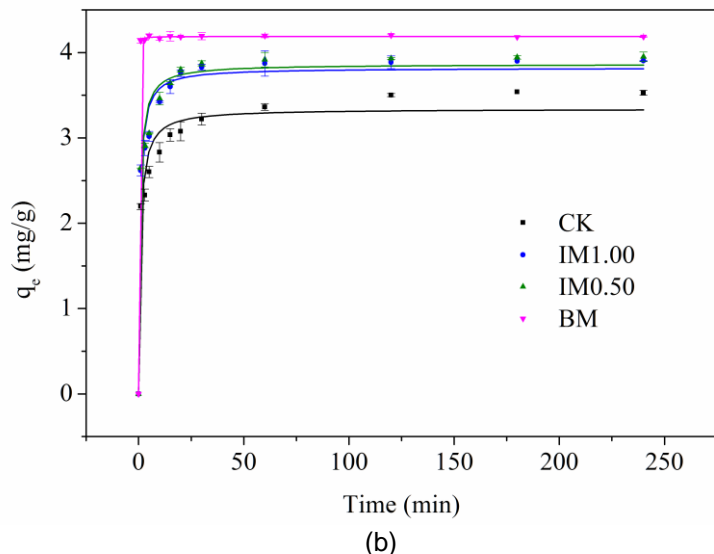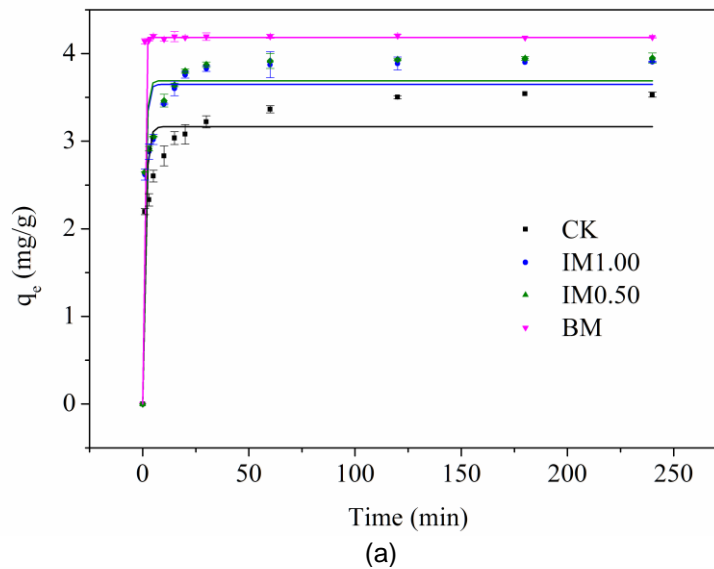
Fig. 7. Adsorption kinetics of of Pb^{2+} onto wheat straw samples at different plant scales: (a) Pseudo-first-order model, (b) Pseudo-second-order model

Table 5. Adsorption Kinetics of of Pb^{2+} onto Wheat Straw Samples at Different Plant Scales

	Pseudo-first-order model			Pseudo-second-order model		
	q_e (mg/g)	K_1 (min^{-1})	R^2	q_e (mg/g)	K_2 (g/(mg·min))	R^2
CK	3.16	0.82	0.86	3.34	0.34	0.95
IM1.00	3.65	1.01	0.91	3.82	0.39	0.97
IM0.50	3.69	1.02	0.91	3.86	0.39	0.98
BM	4.18	4.58	1.00	4.19	17.72	1.00

Adsorption isotherms

The adsorption capacity of Pb^{2+} onto wheat straw samples at different plant scales under different initial Pb^{2+} concentrations is shown in Fig. 8 and Table 6. The adsorption capacity of Pb^{2+} increased with increasing initial Pb^{2+} concentrations. Also, the adsorption capacity of Pb^{2+} increased significantly with decreasing fragmentation scales. The results were consistent with previous research noting that decreasing the median particle size enhanced the adsorption efficiency of Pb^{2+} onto adsorbents (Benhima *et al*. 2008).

It could be concluded from Fig. 9 and Table 7 that the Langmuir and Freundlich isotherms were both applicable to the phenomenon of Pb^{2+} adsorption onto wheat straw; nonetheless, the Langmuir isotherm model fit the experimental data more accurately, which indicated the adsorption mainly occurred in a monolayer. The maximum adsorption capacity of Pb^{2+} onto wheat straw samples (q_m) increased from 37.82 to 42.92 mg/g with decreasing mechanical fragmentation scales. R_L (calculated by K_L) was between 0 and 1, indicating that the adsorption was easy to carry out.

The K_F values of the Freundlich isotherm model increased with decreasing mechanical fragmentation scales, representing a stronger binding force and greater adsorption capacity. $1/n$ values fell between 0.1 and 1, indicating that the adsorption process was prone to occur.
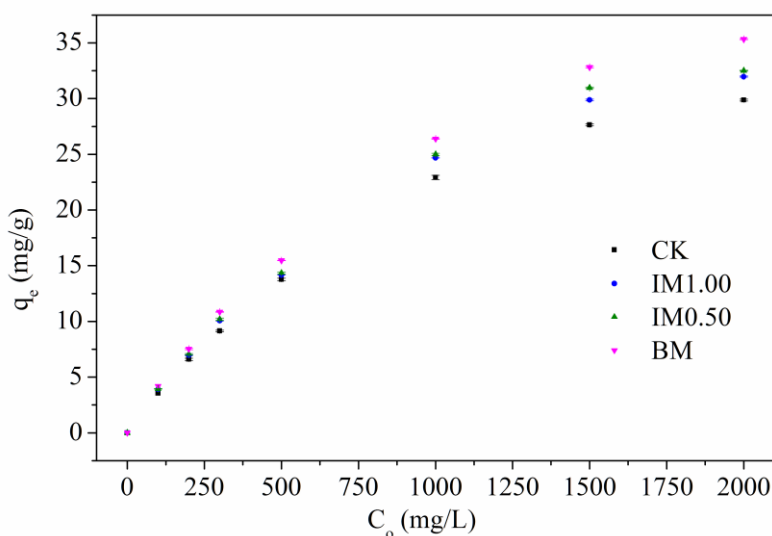
Fig. 8. Adsorption capacity of Pb^{2+} onto wheat straw samples at different plant scales at different initial Pb^{2+} concentrations

Table 6. Adsorption Capacity of Pb^{2+} onto Wheat Straw Samples at Different Plant Scales under Different Initial Pb^{2+} Concentrations

C_o (mg/L)	CK	IM1.00	IM0.50	BM
100	3.54 ± 0.00[a]	3.90 ± 0.00[b]	3.95 ± 0.02[b]	4.18 ± 0.00[c]
200	6.60 ± 0.11[a]	6.97 ± 0.02[b]	7.05 ± 0.06[b]	7.52 ± 0.06[c]
300	9.15 ± 0.06[a]	10.07 ± 0.03[b]	10.20 ± 0.11[b]	10.86 ± 0.02[c]
500	13.75 ± 0.12[a]	14.16 ± 0.01[b]	14.33 ± 0.08[b]	15.47 ± 0.02[c]
1000	22.92 ± 0.20[a]	24.68 ± 0.01[b]	24.99 ± 0.08[c]	26.38 ± 0.04[d]
1500	27.64 ± 0.09[a]	29.88 ± 0.08[b]	30.97 ± 0.06[c]	32.81 ± 0.08[d]
2000	29.87 ± 0.27[a]	31.97 ± 0.24[b]	32.51 ± 0.04[c]	35.33 ± 0.04[d]

Notes: Data are shown as their triplicate mean ± standard deviation.
[a-d] Indicates that values in the same row are significantly different ($p < 0.05$).
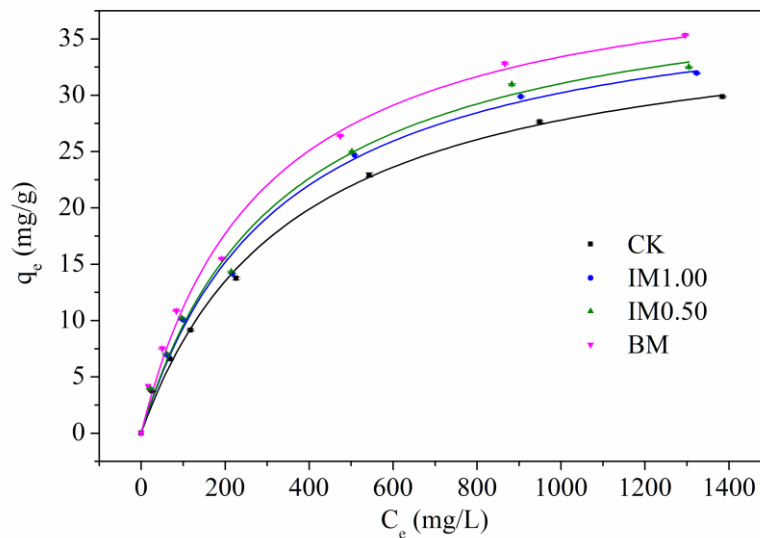
(a)
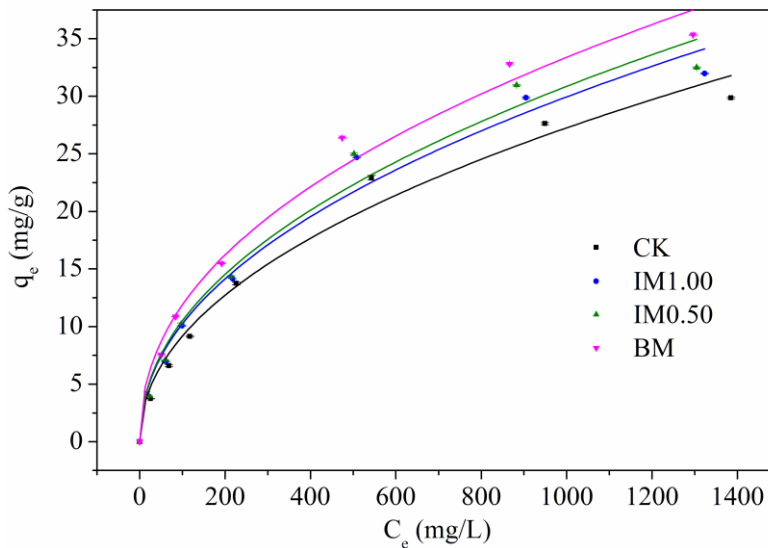
(b)

Fig. 9. Adsorption Isotherms of Pb^{2+} onto wheat straw samples at different plant scales: (a) Langmuir isotherm model, (b) Freundlich isotherm model

bioresources.com

Table 7. Adsorption Isotherms of Pb^{2+} onto Wheat Straw Samples at Different Plant Scales

	Langmuir isotherm model			Freundlich isotherm model		
	q_m (mg/g)	K_L (L/mg)	R^2	$1/n$	K_F (mg/g • (1/mg)$^{1/n}$)	R^2
CK	37.82	0.0027	1.00	0.48	1.04	0.98
IM1.00	40.18	0.0030	0.99	0.47	1.20	0.98
IM0.50	41.30	0.0030	0.99	0.47	1.22	0.98
BM	42.92	0.0035	0.99	0.45	1.51	0.98

Na^+, Mg^{2+}, K^+, and Ca^{2+} released during Pb^{2+} adsorption

As shown in Table 8, the concentrations of Mg^{2+}, K^+ and Ca^{2+} in wheat straw samples at different plant scales showed no significant differences, although Na^+ concentrations decreased after superfine grinding. This indicated that the effect of mechanical fragmentation on the cation concentrations in the wheat straw was limited. The amounts of Na^+, Mg^{2+}, K^+, and Ca^{2+} released did not change significantly between the wheat straw samples at different plant scales, whereas release of Ca^{2+} increased for wheat straw sample at cellular scale. The total amount of cations released showed no significant difference and accounted for about 80% of adsorption capacity of Pb^{2+} onto wheat straw, indicating that ion exchange was the main mechanism, whereby the Ca^{2+} ion exchange was the dominant in the exchangeable process.

Table 8. Changes in Na^+, Mg^{2+}, K^+, and Ca^{2+} Concentrations during Pb^{2+} Adsorption onto Wheat Straw Samples at Different Plant Scales

Cation (meq/g)		CK	IM1.00	IM0.50	BM
Raw straw	Na^+	0.1828 ± 0.0172[b]	0.1543 ± 0.0034[a]	0.1520 ± 0.0025[a]	0.1311 ± 0.0009[a]
	Mg^{2+}	0.0895 ± 0.0016[a]	0.0901 ± 0.0028[a]	0.0909 ± 0.0037[a]	0.0894 ± 0.0000[a]
	K^+	0.5854 ± 0.0480[a]	0.6094 ± 0.0078[a]	0.6224 ± 0.0021[a]	0.5542 ± 0.0422[a]
	Ca^{2+}	0.1346 ± 0.0080[a]	0.1299 ± 0.0011[a]	0.1303 ± 0.0039[a]	0.1387 ± 0.0010[a]
Released	Na^+	0.0036 ± 0.0023[a]	0.0029 ± 0.0018[a]	0.0025 ± 0.0003[a]	0.0017 ± 0.0012[a]
	Mg^{2+}	0.0023 ± 0.0016[a]	0.0045 ± 0.0028[a]	0.0045 ± 0.0030[a]	0.0047 ± 0.0029[a]
	K^+	0.0045 ± 0.0036[a]	0.0032 ± 0.0036[a]	0.0032 ± 0.0036[a]	0.0045 ± 0.0027[a]
	Ca^{2+}	0.0080 ± 0.0017[a]	0.0080 ± 0.0020[a]	0.0085 ± 0.0024[a]	0.0089 ± 0.0029[a]
Total released		0.0287 ± 0.0057[a]	0.0311 ± 0.0114[a]	0.0316 ± 0.0021[a]	0.0335 ± 0.0103[a]

Notes: Data are shown as their duplicate mean ± standard deviation.
[a-b] Indicates that values in the same row are significantly different ($p < 0.05$).

Adsorption Mechanisms of Pb^{2+}

As shown in Table 1, the specific surface areas and pore volumes of wheat straw increased significantly after superfine grinding. SSA values of the cellular-scale sample were nearly four times those of the plant-scale and tissue-scale samples. PV values in the cellular-scale sample were approximately five times larger. Considering that the diameter of Pb^{2+} was 0.238 nm, which was far less than the aperture of wheat samples at different mechanical fragmentation scales, it is speculated that specific surface areas and pore volumes at different mechanical fragmentation scales are not vital parameters for determining the adsorption capacity of Pb^{2+} onto wheat straw samples. In other words, the influence of the mechanical fragmentation scale on physical adsorption was negligible.

The hydroxyl groups of the cellulose chain are important for creating effective complexation interactions with heavy metals (Demirbas, 2008; Al-Ghouti *et al*. 2010). The crystallinity of tissue-scale IM1.00 and IM0.50 samples, and the cellular-scale BM sample

decreased by 13.9%, 15.3%, and 35.8% more than the plant-scale sample CK, respectively. The adsorption capacity of Pb^{2+} increased significantly with decreasing fragmentation scale. On the one hand, cellulose was much more accessible to reagents owing to the reduction of crystallinity, which was beneficial for Pb^{2+} bonding with the adsorption sites (Demirbas, 2008). On the other hand, the hydrogen bonds between hydroxyl in the cellulose chains were broken (Ji *et al*. 2016), and more active hydrogen groups were exposed to participate in the adsorption of heavy metals, thereby improving the adsorption capacity of Pb^{2+}. Moreover, the acidic functional groups contributed to the adsorption efficiency through complexation with heavy metals (Abdolali *et al*. 2014; Salman *et al*. 2015). However, the influence of the mechanical fragmentation scale on the acidic functional groups in wheat straw was not significant, which showed that the fragmentation scale does not affect the complexation of Pb^{2+} by acidic functional groups. It can be concluded that the principal mechanism for improving the adsorption capacity of Pb^{2+} was mainly intensive complexation owing to an increase in cellulose accessibility to water and enhanced chemical reaction activity of the hydroxyl groups.

In addition, the cation exchange capacity (CEC) of wheat straw samples increased notably from plant scale to tissue scale. To some extent, mechanical fragmentation at the tissue scale increased the CEC and improved the cation exchange interaction of Pb^{2+}, thus enhancing the amount of Pb^{2+} adsorption. Nevertheless, the CEC showed no increase at the cellular scale, yet the adsorption efficiency of Pb^{2+} increased significantly. This result can be explained by the fact that the variation of crystallinity was not proportional to the change in Pb^{2+} adsorption capacity; therefore, the mechanism behind this phenomenon requires further intensive study.

CONCLUSIONS

1. Significant differences existed in the median particle size (D_{50}) among wheat straw samples at different plant scales. Due to superfine grinding destroying the tissue and cell wall structures, specific surface areas and pore volumes were significantly higher at cellular scale. The crystallinity declined significantly with decreasing mechanical fragmentation scale as the hydrogen bonds between cellulose chains were broken.

2. The pseudo-second-order kinetic model and the Langmuir isotherm model fit the experimental data better than alternate models. The adsorption capacity of Pb^{2+} was increased significantly with decreasing fragmentation scales. The mechanical fragmentation scale had a negligible influence on physical and electrostatic adsorption. While to a certain extent, the cation exchange interaction of Pb^{2+} was improved by decreasing mechanical fragmentation scale. The principal mechanism improving the adsorption capacity of Pb^{2+} was intensive complexation due to an increase in cellulose accessibility to water and enhanced chemical reaction activity of hydroxyl groups.

ACKNOWLEDGMENTS

REFERENCES CITED

Abdolali, A., Guo, W. S., Ngo, H. H., Chen, S. S., Nguyen, N. C., and Tung, K. L. (2014). "Typical lignocellulosic wastes and by-products for biosorption process in water and wastewater treatment: A critical review," *Bioresource Technol.* 160, 57-66. DOI: 10.1016/j.biortech.2013.12.037

Al-Ghouti, M. A., Li, J., Salamh, Y., Al-Laqtah, N., Walker, G., and Ahmad, M. N. M. (2010). "Adsorption mechanisms of removing heavy metals and dyes from aqueous solution using date pits solid adsorbent," *J. Hazard. Mater.* 176(1-3), 510-520. DOI: 10.1016/j.jhazmat.2009.11.059

Benhima, H., Chiban, M., Sinan, F., Seta, P., and Persin, M. (2008). "Removal of lead and cadmium ions from aqueous solution by adsorption onto micro-particles of dry plants," *Colloid. Surface. B.* 61(1), 10-16. DOI: 10.1016/j.colsurfb.2007.06.024

Boehm, H. P. (1966). "Chemical identification of surface groups," *Adv. Catal.* 16, 179-274.

Dang, V. B. H., Doan, H. D., Dang-Vu, T., and Lohi, A. (2009). "Equilibrium and kinetics of biosorption of cadmium (II) and copper (II) ions by wheat straw," *Bioresource Technol.* 100(1), 211-219. DOI: 10.1016/j.biortech.2008.05.031

Demirbas, A. (2008). "Heavy metal adsorption onto agro-based waste materials: A review," *J. Hazard. Mater.* 157(2-3), 220-229. DOI: 10.1016/j.jhazmat.2008.01.024

Ding, Y., Jing, D., Gong, H., Zhou, L., and Yang, X. (2012). "Biosorption of aquatic cadmium (II) by unmodified rice straw," *Bioresource Technol.* 114, 20-25. DOI: 10.1016/j.biortech.2012.01.110

Farooq, U., Khan, M. A., Athar, M., and Kozinski, J. A. (2011). "Effect of modification of environmentally friendly biosorbent wheat (*Triticum aestivum*) on the biosorptive removal of cadmium (II) ions from aqueous solution," *Chem. Eng. J.* 171(2), 400-410. DOI: 10.1016/j.cej.2011.03.094

Farooq, U., Kozinski, J. A., Khan, M. A., and Athar, M. (2010). "Biosorption of heavy metal ions using wheat based biosorbents – A review of the recent literature," *Bioresource Technol.* 101(14), 5043-5053. DOI: 10.1016/j.biortech.2010.02.030

Feng, N., Guo, X., and Liang, S. (2009). "Adsorption study of copper (II) by chemically modified orange peel," *J. Hazard. Mater.* 164(2-3), 1286-1292. DOI: 10.1016/j.jhazmat.2008.09.096

Fomina, M., and Gadd, G. M. (2014). "Biosorption: Current perspectives on concept, definition and application," *Bioresource Technol.* 160, 3-14. DOI: 10.1016/j.biortech.2013.12.102

Gao, C., Xiao, W., Ji, G., Zhang, Y., Cao, Y., and Han, L. (2017). "Regularity and mechanism of wheat straw properties change in ball milling process at cellular scale," *Bioresource Technol.* 241, 214-219. DOI: 10.1016/j.biortech.2017.04.115

Gong, C., Huang, J., Feng, C., Wang, G., Tabil, L., and Wang, D. (2016). "Effects and mechanism of ball milling on torrefaction of pine sawdust," *Bioresource Technol.* 214, 242-247. DOI: 10.1016/j.biortech.2016.04.062

Gorgievski, M., Božić, D., Stanković, V., Štrbac, N., and Šerbula, S. (2013). "Kinetics, equilibrium and mechanism of Cu^{2+}, Ni^{2+} and Zn^{2+} ions biosorption using wheat straw," *Ecol. Eng.* 58, 113-122. DOI: 10.1016/j.ecoleng.2013.06.025

Gupta, V. K., Shrivastava, A. K., and Jain, N. (2001). "Biosorption of chromium (VI) from aqueous solutions by green algae *Spirogyra* species," *Water Res.* 35(17), 4079-4085. DOI: 10.1016/S0043-1354(01)00138-5

Himmelsbach, D. S., Khalili, S., and Akin, D. E. (2002). "The use of FT-IR microspectroscopic mapping to study the effects of enzymatic retting of flax (*Linum usitatissimum L*) stems," *J. Sci. Food Agr.* 82, 685-696. DOI:10.1002/jsfa.1090

Hubbe, M. A., Hasan, S. H., and Ducoste, J. J. (2011). "Cellulosic substrates for removal of pollutants from aqueous systems: A review. 1. Metals," *BioResources* 6(2), 2161-2287. DOI: 10.15376/biores.6.2.2161-2287

Ibrahim, M. M., El-Zawawy, W. K., Abdel-Fattah, Y. R., Soliman, N. A., and Agblevor, F. A. (2011). "Comparison of alkaline pulping with steam explosion for glucose production from rice straw," *Carbohyd. Polym.* 83, 720-726. DOI:10.1016/j.carbpol.2010.08.046

Ji, G., Gao, C., Xiao, W., and Han, L. (2016). "Mechanical fragmentation of corncob at different plant scales: Impact and mechanism on microstructure features and enzymatic hydrolysis," *Bioresource Technol.* 205, 159-165. DOI: 10.1016/j.biortech.2016.01.029

Kalavathy, M. H., and Miranda, L. R. (2010). "Comparison of copper adsorption from aqueous solution using modified and unmodified *Hevea brasiliensis* saw dust," *Desalination* 255(1-3), 165-174. DOI: 10.1016/j.desal.2009.12.028

Liu, Z., Qin, L., Pang, F., Jin, M., Li, B., Kang, Y., Dale, B. E., and Yuan, Y. (2013). "Effects of biomass particle size on steam explosion pretreatment performance for improving the enzyme digestibility of corn stover," *Ind. Crop. Prod.* 44, 176-184. DOI:10.1016/j.indcrop.2012.11.009

Mishra, V., Balomajumder, C., and Agarwal, V. K. (2010). "Biosorption of Zn (II) onto the surface of non-living biomasses: A comparative study of adsorbent particle size and removal capacity of three different biomasses," *Water, Air, & Soil Pollution* 211(1-4), 489-500. DOI: 10.1007/s11270-009-0317-0

Pandi, K., and Viswanathan, N. (2015). "A novel metal coordination enabled in carboxylated alginic acid for effective fluoride removal," *Carbohydr. Polym.* 118, 242-249. DOI: 10.1016/j.carbpol.2014.10.068

Rao, M. M., Rao, G. P. C., Seshaiah, K., Choudary, N. V., and Wang, M. C. (2008). "Activated carbon from *Ceiba pentandra* hulls, an agricultural waste, as an adsorbent in the removal of lead and zinc from aqueous solutions," *Waste Manage.* 28(5), 849-858. DOI: 10.1016/j.wasman.2007.01.017

Robalds, A., Naja, G. M., and Klavins, M. (2016). "Highlighting inconsistencies regarding metal biosorption," *J. Hazard. Mater.* 304, 553-556. DOI: 10.1016/j.jhazmat.2015.10.042

Salman, M., Athar, M., and Farooq, U. (2015). "Biosorption of heavy metals from aqueous solutions using indigenous and modified lignocellulosic materials," *Rev. Environ. Sci. Bio.* 14(2), 211-228. DOI: 10.1007/s11157-015-9362-x

Segal, L., Creely, J. J., Martin Jr., A. E., and Conrad, C. M. (1959). "An empirical method for estimating the degree of crystallinity of native cellulose using the X-ray diffractometer," *Text. Res. J.* 29(10), 786-794. DOI: 10.1177/004051755902901003

Shen, Z., Zhang, Y., McMillan, O., Jin, F., and Al-Tabbaa, A. (2017). "Characteristics and mechanisms of nickel adsorption on biochars produced from wheat straw pellets and rice husk," *Environ. Sci. Pollut. R.* 24(14), 12809-12819. DOI: 10.1007/s11356-017-8847-2

Silva, G. G. D., Couturier, M., Berrin, J., Buléon, A., and Rouau, X. (2012). "Effects of grinding processes on enzymatic degradation of wheat straw," *Bioresource Technol.* 103(1), 192-200. DOI: 10.1016/j.biortech.2011.09.073

Sluiter, J. B., Ruiz, R. O., Scarlata, C. J., Sluiter, A. D., and Templeton, D. W. (2010). "Compositional analysis of lignocellulosic feedstocks. 1. Review and description of methods," *J. Agr. Food Chem.* 58(16), 9043-9053. DOI: 10.1021/jf1008023

Tan, G., and Xiao, D. (2009). "Adsorption of cadmium ion from aqueous solution by ground wheat stems," *J. Hazard. Mater.* 164(2-3), 1359-1363. DOI: 10.1016/j.jhazmat.2008.09.082

Wang, F., Liang, J., Tang, Q., Chen, C., and Chen, Y. (2014). "Channel microstructure and thermal insulation mechanism of sepiolite mineral nanofibers," *J. Nanosci. Nanotechno.* 14(5), 3937-3942. DOI: 10.1166/jnn.2014.7982

Wang, Z., Liu, G., Zheng, H., Li, F., Ngo, H. H., Guo, W., Liu, C., Chen, L., and Xing, B. (2015). "Investigating the mechanisms of biochar's removal of lead from solution," *Bioresource Technol.* 177, 308-317. DOI: 10.1016/j.biortech.2014.11.077

Yuan, Z., Long, J., Wang, T., Shu, R., Zhang, Q., and Ma, L. (2015). "Process intensification effect of ball milling on the hydrothermal pretreatment for corn straw enzymolysis," *Energ. Convers. Manage.* 101, 481-488. DOI:10.1016/j.enconman.2015.05.057

Zhang, H., Chen, L., Lu, M., Li, J., and Han, L. (2016). "A novel film–pore–surface diffusion model to explain the enhanced enzyme adsorption of corn stover pretreated by ultrafine grinding," *Biotechnol. Biofuels* 9(1). DOI: 10.1186/s13068-016-0602-2

Zhang, Y., Xiao, W., Ji, G., Gao, C., Chen, X., Cao, Y., and Han, L. (2017). "Effects of multiscale-mechanical grinding process on physicochemical properties of black tea particles and their water extracts," *Food Bioprod. Process.* 105, 171-178. DOI: 10.1016/j.fbp.2017.05.002